

CONTACT STRESS ANALYSIS OF WHEEL-RAIL FOR DIFFERENT WHEEL-RAIL PROFILES USING FINITE ELEMENT ANALYSIS

Peddinti Nehemiah

*Professor, Faculty of Mechanical and Industrial Engineering, Bahir Dar Institute of
Technology, Bahir Dar University, Ethiopia.*

Abstract

Operation of railway transportation depends on wheel and rail which support and guide the railway vehicle safely and smoothly. Due to the applied load on the wheel, contact stress is developed between the wheel and rail which leads to wear, deformation and damage of these parts resulting in more cost to maintain or replace. This study aims primarily at the determination of stresses by varying contact geometry arising from variation in profile geometry such as; rail profile radii, wheel profile radii and wheel profile taper. To analyze the influence of profile geometry seven different values of profile radii are chosen for wheel R7T and rail UIC60 selected materials as per European Norm/Standard. The methods used are Hertzian Contact method and Finite Element Method (FEM) to calculate contact stresses and maximum contact pressure. A three-dimensional finite element model for wheel-rail is developed and load is applied to determine the stress at the contact patch. It is observed that the magnitudes of equivalent stress are 338.29 MPa from FEA and 333.31 MPa from Hertzian Contact Theory (HCT) for the wheel radius of 330 mm and the rail radius of 300 mm. Similarly, for wheel and rail radii of curvature 360 mm and 300 mm the values of equivalent stress are 329.67 MPa from FEA and 324.28 MPa from HCT. When the results of two methods HCT and FEA are compared they agree well with each other with the maximum deviation of 2.29%. This percentage of error may be due to the assumptions made in Hertzian contact theory during the analysis. This research work may help in designing the application for railways.

Keywords: HCT, Kalker's Contact Theory, FEA, Wheel-rail Profile radii, Contact stress, Contact pressure

Introduction

Many researchers have determined the Contact stresses developed during the pressing action of wheel and rail in the past research. Vahid Monfared [1] presented the contact stress analysis in rolling bodies using finite element method (FEM) to analyze the contact pressure of wheel and rail, assuming the contact surfaces as elliptical, rectangular and circular. The results of contact stress with assumption of elliptical contact surface were similar to the exact

analytical results than the contact stress results obtained by assumption of rectangular and circular contact surface. Satish et. al [2] studied the performance analysis of wheel and rail contact based on different values of Young's modulus and yield strength ratio (E/Y). From the simulation results of wheel and rail contact model the maximum stress and strain values were at the edge of the contact for low E/Y value of material and at the center point for high E/Y value of material. Peter Tamas, et al [3] proposed the frictional contact analysis of wheel-rail to compare the contact behavior of wheel-rail contact during stationary, sticking sliding conditions using FEM by calculating the contact pressure distribution, contact area and equivalent von Mises stress distribution. Srivastava, et al [4] studied the influence of interacting wheel and rail profile topology for standard UIC60 material based on the contact stress analysis in wheel-rail by Hertzian method and FEM. The analytical formulation is based on Timoshenko's approach and FEM based simulation is under taken to obtain the distribution of contact zones, contact stress and contact pressure for different configuration of the wheel and rail profiles. Sunil Kumar Sharma, et al [5] carried out the research on the dynamic contact analysis of standard wheel and rail UIC60 as per standards of Indian railways using Quasi-Hertz and FEA to analyze the impact of the interacting wheel and rail profiles on the distribution of contact zones and stresses. Kalker's theory was also used in this study to find the effect of lateral movement in the evolution of frictional forces, which alters both the shape of rail contact area and the pressure distribution. Aleksander Sladkowski and Marek Sitarz [6] presented the analysis of wheel-rail interaction using FE software and the Quasi-Hertz method as basis for mathematical simulation. As a result of their research, distribution of contact zones and stresses for various wheel and rail profiles have been determined. Sowndarya and Ratna Kiran [7] established a FEM model of rail and wheel interaction using dynamic stress analysis in order to evaluate maximum contact pressure, stress, strain and the contact forces by considering a real condition of wheel and rail including boundary and loading conditions. Natsumi and Yoshiaki [8] proposed a coupled train model with a multibody system considering three-dimensional wheel/rail contact geometry to assess the safety of high-speed railway vehicles. As railway vehicles are becoming lighter and are running at high speeds it is necessary to discuss their safety when subjected to a crosswind. In their research they used the proposed model in a situation presupposing strong crosswinds in order to analyze the behavior of coupled trains under this condition. They discussed the modeling and formulation of a coupled train as well as wheel unloading ratios. The results showed that the vibration of a car body was the largest in the wheel unloading ratios of the

car body when the frequency of the car body was close to the second-mode natural frequency of the vehicle system.

Sajjad Z et al [9] discussed the evolution and the current state of the theories for solving the wheel–rail contact problem for rolling stock. The well-known theories for modelling both normal contact (Hertzian and non-Hertzian) and tangential contact (Kalker's linear theory, FASTSIM, CONTACT, Polach's theory, etc.) were reviewed. The authors focused on simplifying assumptions for developing these models and comparing their functionality. The experimental studies for evaluation of contact models were also reviewed. The Rolling contact fatigue (RCF) damage of high-speed wheels is a main factor that affects railway safety. Qian et al. [10] presented a Finite element model (FEM) of high-speed transient rolling contact that considers kinetic parameters as initial conditions. This model was used to calculate wheel/rail RCF. With a CRH2 high-speed train as the research object, a head car model was established with the multibody dynamics software UM. The train was driven on a straight track at a speed of 300 km/h. Different contact geometric parameters, such as lateral displacement and attack angle, were obtained. A 3D high-speed transient elastic-plastic FEM of wheel/rail rolling contact was then developed by using ABAQUS with the initial dynamic contact geometric parameters. The actual geometries of the wheel tread and rail head as well as the elastic-plastic properties were considered in this model. This consideration makes the model highly suitable for solving 3D transient rolling contact behavior. The normal force, creep force, and contact area in the contact patch were solved and used in the fatigue model. The maximum speed of a high-speed train was limited to its critical speed. Yeon- and Bum [11] in their research reviewed the definition of critical speed, the relationship between creepage and creep force and the effects of the parameters of the first and second suspension systems were also studied using a bogie model to increase the critical speed. Kalker's linear creep theory and its modification of Wormey's saturation constant were reviewed. Flange contact was also considered when lateral displacement exceeds the dead band between wheel flange and rail. Direct numerical integration and a shooting algorithm were devised to calculate the response. Results showed that as speed increases, the equilibrium point becomes unstable and creates a limit cycle through a Hopf bifurcation. The unstable fixed point can be a critical speed. The critical speed increases as the creep curve becomes stiff before saturation, which is more effective than the variation in suspension parameters.

Oldrich Polach and Dirk Nicklisch [12] presented the dynamic behavior of railway vehicles considering the wheel/rail contact geometry parameters, equivalent conicity and profile

alteration due to wear with increasing running distance as well as their relationship. The results showed that the equivalent conicity increases while the non-linearity parameter decreases with increasing vehicle mileage. Roya Sadat Ashofteh and Ali Mohammaddnia [13] studied the stress analysis in the elastic-plastic analysis of railways using ABAQUS for U33 and UIC60 rails type of materials and the R7T wheels type of material by assuming both wheel and rail under static loading. The FEM modeling result was within the elastic range. But, under dynamic load due to high forces applied and stresses exceeding the yield stress, the wheel material behavior was within elastic-plastic limit. Yuewei Ma, et al. [14] worked on the verification of FE model against CONTACT software and to explore the effect of most influencing factors on the tribological behavior of wheel-rail interaction through parametric studies using this model. The comparison of FE model and CONTACT model was carried out for the results of shear stress, normal contact pressure, and slip-adhesion area. In this study, the influence of varying operational patterns (such as frictional coefficient and traction forces) on the surface and subsurface tribological responses of wheel-rail interaction was accomplished using finite element model. According to Lewis [15] a steel wheel rolling on steel rails is the principal characteristic that distinguishes railways from other forms of transport. Wheel and rail meet at a contact patch that is small and carries the full wheel load through which all steering, traction, and braking forces are transmitted. The contacts usually act as stress concentrations, and are thus probable locations for mechanical failure.

From the above-surveyed literature, it is found that no researchers have carried out contact stress analysis for R7T wheel material and UIC60 for rail material by using different wheel profile radii, rail profile radii and wheel taper profile, and this lacking in the scientific literature is taken as our present work. Srivastava, et al [6], used a radius of wheel 1098 mm and the material for both wheel and rail is UIC60. Whereas, in our research work the radius of the wheel is taken as 460 mm and R7T as wheel material and

UIC60 as rail material, and the contact stress analysis is carried out by Hertzian contact theory and FEA.

STRESS ANALYSIS OF WHEEL-RAIL CONTACT: In the 1880s, Hertz developed his influential work on contact mechanics, to calculate the contact area and the normal pressure distribution between the contact bodies. The K. L. Johnson [16], further used Hertzian Contact Theory (HCT) to develop the contacts between two solids. He proved that when two elastic non-conforming solids are brought into contact the HCT can be applied for modeling

the contact between wheel and rail assuming elliptical shape for the contact area and a semi-ellipsoid contact pressure distribution in the contact region. The distance between each contacting surface is given by:

$$z_1 = A_1x^2 + B_1y^2 \tag{1}$$

$$z_2 = A_2x^2 + B_2y^2 \tag{2}$$

As the contacting surfaces of the bodies before loading are represented by $z_1(x, y)$ and $z_2(x, y)$ for the first and the second body, respectively.

The total distance between the undeformed surfaces (before loading), $z = |z_1| + |z_2|$, is given as:

$$z(x, y) = Ax^2 + By^2 \tag{3}$$

From wheel-rail configuration the radii curvatures are related as;

$$A + B = \frac{1}{2} \left(\frac{1}{R_1^r} + \frac{1}{R_1^t} + \frac{1}{R_2^r} + \frac{1}{R_2^t} \right) \tag{4}$$

$$|B - A| = \frac{1}{2} \left[\left(\frac{1}{R_1^r} - \frac{1}{R_1^t} \right)^2 + \left(\frac{1}{R_2^r} - \frac{1}{R_2^t} \right)^2 + 2 \left(\frac{1}{R_1^r} - \frac{1}{R_1^t} \right) \left(\frac{1}{R_2^r} - \frac{1}{R_2^t} \right) \cos 2\psi \right]^{1/2} \tag{5}$$

Where A and B are geometrical constants, R_1^r , R_1^t , R_2^r and R_2^t are radii of curvatures of the profile as shown in figure 1, and ψ is the angle between the normal planes of the radii of curvatures. The constants A and B depend on the magnitudes of the principal curvatures of the surfaces in contact and on the angle between the planes of principal curvatures of the two surfaces ‘ θ ’. This angle is given by:

$$\cos \theta = \frac{|B-A|}{A+B} \tag{6}$$

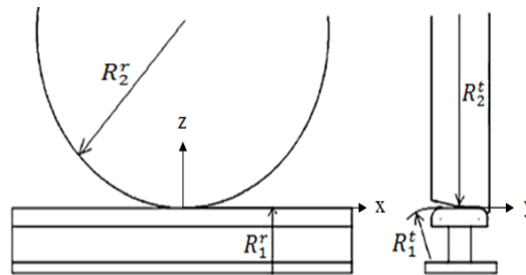


Fig.1 Wheel–rail configuration showing different principal relative radii of curvature

Where,

R_1^r - The radius of the rail along rolling which is infinity in this case

R_1^t - The transverse radius of curvature of the rail profile, in the plane of cross section

R_2^r - The rolling radius of curvature of the wheel.

R_2^t -The transverse radius of curvature of the wheel profile in the plane of cross section which goes to infinity for a conical wheel, and

ψ - conicity (wheel taper angle)

The ratio $g = b/a = n/m$ can also be approximated to solve the tangential contact problem directly as:

$$\frac{b}{a} = \frac{n}{m} \approx \left(\frac{A}{B}\right)^{0.63} \quad (7)$$

The pressure distribution is given by:

$$P = P_o \left(1 - \frac{x^2}{a^2} - \frac{y^2}{b^2}\right)^{1/2}, \quad |x| \leq a, |y| \leq b \quad (8)$$

Where, P_o is the maximum contact pressure at the first point of contact, ‘a’ is semi-major axis and ‘b’ is semi-minor axis.

Therefore, the maximum pressure, P_o is related to the prescribed contact force/normal force, F , through:

$$P_o = \frac{3F}{2\pi ab} \quad (9)$$

The semi axes of the elliptic boundary of the surface of contact ‘a’, ‘b’ and the reduction of the distance between the bodies’ after contact at the centers called approach ‘ δ ’ are given by:

$$a = m \left[\frac{3F}{4E^*} \frac{1}{A+B}\right]^{1/3} \quad (10)$$

$$b = n \left[\frac{3F}{4E^*} \frac{1}{A+B}\right]^{1/3} \quad (11)$$

$$\delta = r \left[\left(\frac{3F}{4E^*}\right)^2 (A + B)\right]^{1/3} \quad (12)$$

Where,

$$\frac{1}{E^*} = \frac{1-\nu_1^2}{E_1} + \frac{1-\nu_2^2}{E_2} \quad (13)$$

With E_1, E_2 and ν_1, ν_2 are being the elastic modules and Poisson ratios of the bodies in contact respectively.

The non-dimensional values of m and n for different values of angle θ are given in table 1.

Timoshenko [17], developed the equations to calculate principal stresses at the surface of contact. Considering points on the elliptical surface of contact and taking the x- and y-axes in the direction of semi-axis ‘a’ and ‘b’ respectively, the principal stresses at the center of the surface of contact are:

$$\sigma_x = -2\nu P_o - (1 - 2\nu)P_o \frac{b}{a+b} \quad (14)$$

$$\sigma_y = -2\nu P_o - (1 - 2\nu)P_o \frac{a}{a+b} \quad (15)$$

$$\sigma_z = -P_0 \tag{16}$$

Where; σ_x , σ_y and σ_z are the stress components along x, y and z axis respectively.

Distortion Energy Theory: Budynas-Nisbett [18], developed the distortion-energy theory to predict the equivalent von Mises stress for the general three-dimensional states of stress σ_x , σ_y and σ_z which is given by:

$$\sigma' = \left[\frac{(\sigma_x - \sigma_y)^2 + (\sigma_y - \sigma_z)^2 + (\sigma_z - \sigma_x)^2}{2} \right]^{1/2} \tag{17}$$

According to this theory, yielding occurs when the von Mises stress exceeds or equals to the yield strength. That means:

$$\sigma' \geq S_y \tag{18}$$

Dimension of Wheel and Rail Geometries: The dimensions of wheel and rail used in this research are selected depending on European Standard (EN) and the European Union standards for railways UIC60-1 respectively. According to these standards the wheel material R7T plain carbon steel with S1002 wheel profile (contact phase) construction is selected and UIC60 is used for the rail part with 1 in 40 rail inclination. As shown in figure 2, the rail contact profile has three circular arcs which are faces exposed to contact depending on the position of the wheel movement. From the three circular arcs contact may happen mostly at 300 mm profile of rail. Hence, this radius of contact profile is changed for seven different values from 270 mm to 330 mm profile radii to determine the contact stresses due to this profile changes. Similarly, the wheel profile has also three circular contact zones 13 mm, 100 mm and 330 mm with taper profile 5% as shown in figure 3. Here also the profile radius 330 mm is varied from 300 mm to 360 mm and wheel profile taper is changed from 1 in 5 to 1 in 35 for seven different values.

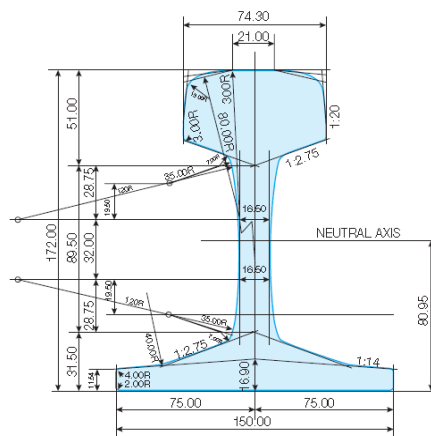


Fig. 2 UIC60 rail profile

(Source: Nippon Steel and Sumitomo Metal Corporation, Tokyo 2014 [19])

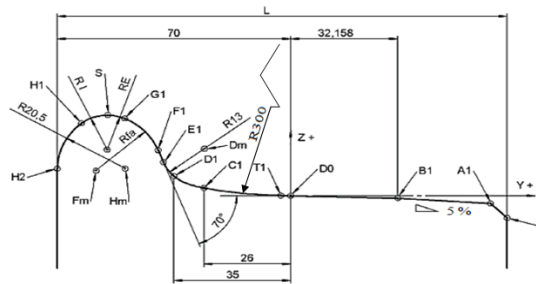


Fig.3 S1002 Wheel Contact Phase Profile (Source: PR NF EN 13715, European Standard, 2015 [20])

Generally, depending on the above standards we have the following properties for wheel-rail materials.

Contact load, $F = 83000 \text{ N}$

Young's modulus of elasticity $E_1 = 210 \text{ GPa}$ for rail

Young's modulus of elasticity $E_2 = 200 \text{ Gpa}$ for wheel

Poisson's ratio $\nu_1 = \nu_2 = 0.3$ for both rail and wheel

Ultimate tensile strength $\sigma_{ut} = 960 \text{ MPa}$ for rail and $\sigma_{ut} = 880 \text{ MPa}$ for wheel

Yield strength $\sigma_y = 0.5\sigma_{ut}$ for both wheel and rail

Rolling radius curvature of wheel, $R_2^r = 460 \text{ mm}$

The maximum operational speed of the train = 80 Km/hr

Axle load is <17

The mass of the wheel = 412 kg

The total weight of the wheel = 83 KN

Finite Element Analysis: The assembled three-dimensional analysis of wheel-rail contact model aims to study the contact stress for different profiles. 3D geometrical modeling of wheel and rail is carried out in a Solid Work 15 environment including their assemblies as shown in figure 4. Mostly the distance between two bogies that supports the rail from the bottom is 600 mm. Considering two bogies in this paper rail is modeled with restriction to an overall length of 1200 mm.

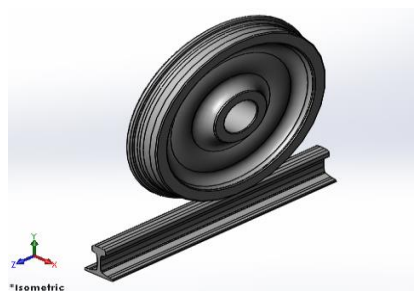


Fig.4 Assembly of wheel and rail using solid work

The 3D model is imported to ANSYS work-bench 15 through geometry and the mesh is generated with fine mesh as shown in figure 5. Under connections the contact type is frictional with a coefficient of friction 0.3 at the interface between wheel and rail in order to predict tangential frictional force, having symmetrical behavior with Augmented Lagrange formulation. The face sizing is used in the contact region to have good contact results with element size 3 mm. After meshing the FE model has 183284 elements and 311450 nodes as a maximum value.

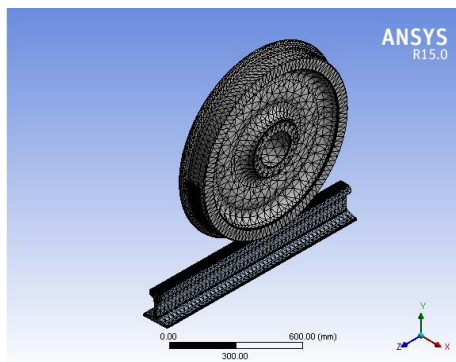


Fig.5 Finite element model and meshing system of wheel and rail

Under static structural boundary conditions are inserted as shown in figure 6. Under solution, the equivalent stress/von-Mises stress and contact tool (pressure) are inserted to evaluate the results.

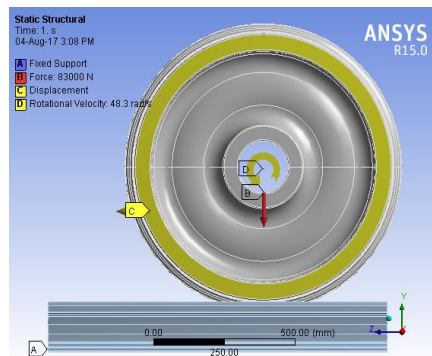


Fig.6 Loading condition

RESULTS AND DISCUSSION

The analyses are carried out by using Hertz contact theory and FEA. The effect of geometrical parameters (WPT, wheel profile radii, and rail profile radii) for different contact parameters like semi-major axis 'a', semi-minor axis 'b', maximum contact pressure 'p_o', principal stresses and equivalent von Mises stress 'σ'' are calculated using equations (1 - 17).

Table 2 presents the analytical results showing the effect of variation in wheel profile taper (conicity) designated as ψ , reduction in this conicity causes very slight increase in the von Mises stress and a decrease in the maximum contact pressure. It can be seen from this table there are no such much differences on the semi-axes as the conicity is decreasing, that means the contact area (πab) is nearly equal for all cases. Since as the wheel profile taper increases sliding friction becomes higher but in this case, the conicity shows no such variations on the values of maximum contact pressure and von Mises stresses. This implies that the wheel profile taper has less effect on the contact stresses.

Table 3 shows the effect of change of rail profile radii on the contact parameters such as maximum contact pressure, stress components and von Mises stress. These parameters depend on non-dimensional coefficients m and n with the profile radii. Due to small variations between the minimum and maximum values of these non-dimensional coefficients slight magnitude change is occurring in the parameters. As rail profile radii increase the contact patch length decreases and width of the elliptical contact patch increases for the interval of 270 mm to 330 mm rail profile radii. Hence, by increasing rail profile radii von Mises stress and maximum contact pressure become less. Even though there is a change in magnitude the percentage in the difference between the minimum and maximum values of these contact pressures and von Mises stresses are less than 5% for both methods HCT and FEA. A Similar trend is observed with varying the radii of curvature of wheel profile tabulated in table 4 for contact dimensions. Here also as the wheel profile radii increase the maximum contact pressure and von Mises stress slight decrements in both methods HCT and FEA. Therefore, in this case, the effect of change of radius of curvature of both rail and wheel has a less significant effect on the contact stresses created between wheel and rail.

From the results obtained in tables 3 and 4, the Hertz's normal contact theory coincide well with that of the FEA which have less than 1.63% difference for maximum contact pressure and 2.29% for equivalent stresses. This percentage difference may be due to the assumptions used in case of Hertzian contact theory and Tangential contact theory.

Figures 7 and 8 demonstrate the values von Mises stress and maximum contact pressure of the contact between rail 300 mm with wheel 330 mm profile radius respectively and by changing profile radii for each wheel and rail the values are summarized in table 3 and 4 for both Hertzian contact analysis and FEA.

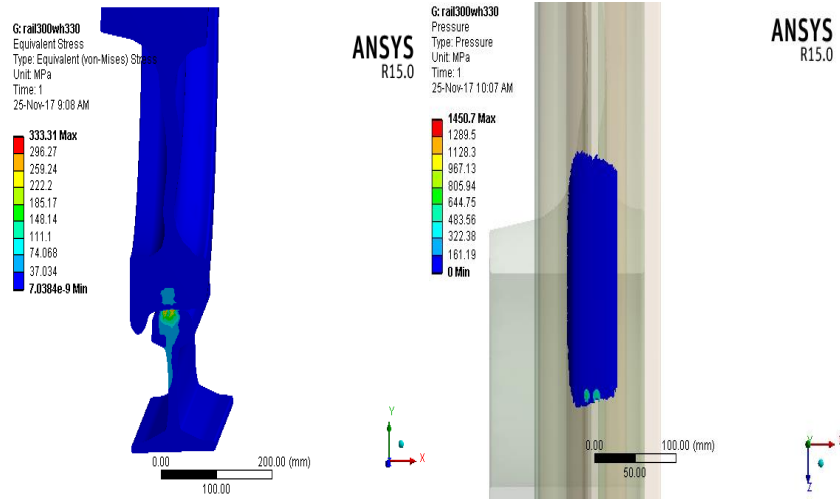


Fig.7 Equivalent stress for rail 300 mm and 330mm wheel profiles

Fig.8 Maximum contact pressure for rail 300 mm and 330mm wheel profiles.

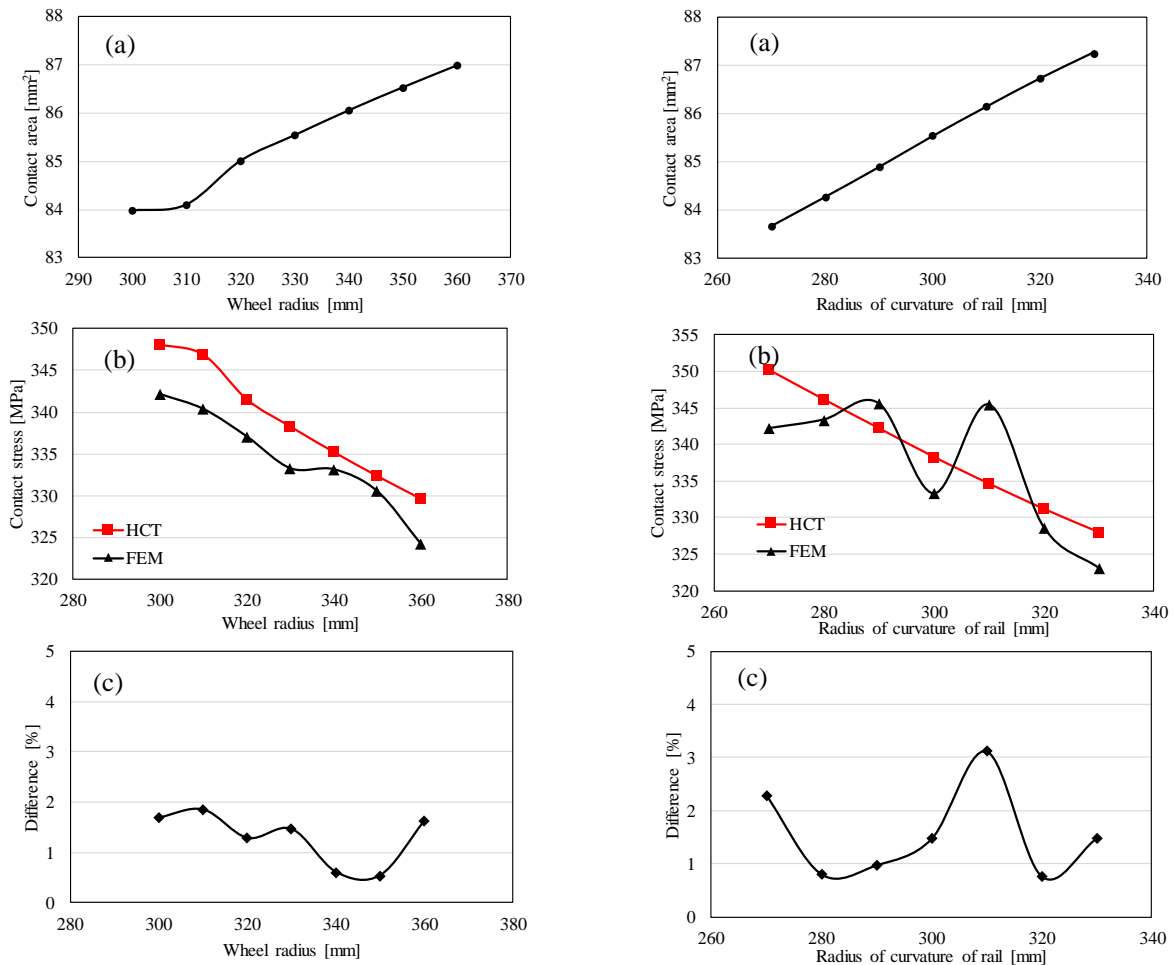


Fig.9 a) Contact area Vs Wheel radius. b) Contact stress Vs Wheel radius. c) Difference (%) Vs Wheel radius.

Fig.10 a) Contact area Vs radius of curvature b) Contact stress Vs radius of curvature c) Difference(%)Vs radius of curvature.

Conclusion

In this research work, contact stresses between wheel and rail are determined by varying contact profile geometries using Hertzian contact theory and FEA, the results of which are believed to be significant. The analysis includes contact dimension, von Mises stress and maximum contact pressure of the wheel-rail when a vertical load is applied at the center of the wheel. The fatigue life analysis is also done using tangential contact theory and FEA when the tangential and vertical load is applied at the contact point of wheel-rail. From the results obtained in the analysis, the following can be concluded.

The results obtained by varying Wheel Profile Taper (WPT) on contact dimension, maximum contact pressure, and von Mises stress are almost similar for 1 in 5 to 1 in 35 intervals. This implies that the variations of WPT have less significant effects on the contact stresses. So we can use one value from the interval for only the analysis of contact stresses using Hertzian contact theory.

The effect of changing the radius of curvature of wheel and rail on elliptical contact patch size, maximum contact pressure, and equivalent stress shows slight variations for the interval of 300 mm to 360 mm for wheel and 270 mm to 330 mm rail profile radii for both HCT and FEA methods. Additionally, as this radius of curvatures of both wheel and rail increases the longitudinal and lateral creep forces small increment, resulting in a fewer increase in coefficient of traction that causes sliding friction to increase.

Based on Hertzian contact theory and FEA contact pressure values for S1002 wheel and UIC60 rail profiles are determined. From the results, it can be seen that the maximum difference between the two methods in percentage is 2.29% and from tangential contact theory and FEA the maximum percentage difference is 12.8%. The deviation in the result can be attributed to the assumptions made in the Hertzian contact theory and tangential contact theory.

References:

- Vahid Monfared, "Contact Stress Analysis in Rolling Bodies by Finite Element Method (FEM) Statically", *Journal of Mechanical Engineering and Automation* 2012, 2(2) pp. 12-16.
- V. C. Sathish Gandhi, R. Kumaravelan, S. Ramesh, M. Thanmanaselvi, K. Sriram, "Performance Analysis of Wheel and Rail Contact by Nature of Material Characteristics", *Mechanics and Mechanical Engineering* Vol. 18, No. 1 (2014), pp. 11-24.

- Péter Tamás Zwierczyk and Károly Váradi, "Frictional contact FE analysis in a railway wheel-rail contact", *Periodica Polytechnica Mechanical Engineering*, 15 April 2014, 58(2), pp. 93 - 99.
- J. P. Srivastava, P. K. Sarkar, V. Ranjan, "Contact Stress Analysis in Wheel–Rail by Hertzian Method and Finite Element Method", *Journal of Institution of Engineers (India) Series C*, October–December 2014, pp. 319-325.
- Sunil Kumar Sharma, Anil Kumar, "Dynamics Analysis of Wheel-Rail Contact Using FEA", 12th International Conference on Vibration Problems, ICOVP 2015, pp. 1119-1128.
- Aleksander Sladkowski*, Marek Sitarz, "Analysis of wheel-rail interaction using FE software", *Wear* 258 (2005) pp. 1217–1223.
- M. V. Sowndarya, V. Ratna Kiran, "Dynamic Contact Analysis of Wheel and Rail Mechanism for Obtaining Maximum Contact Pressure", *International Journal of Engineering Research & Technology (IJERT)*, Vol. 4 Issue 07, July-2015 pp. 2278-2281.
- Natsumi Nakano and Yoshiaki Terumichi, "Numerical Analysis for Coupled Train Considering 3D Wheel/Rail Contact Geometry", *Journal of Mechanical Science and Technology*, Vol. 29, No. 7 (2015), pp. 2677-2683.
- Sajjad Z. Meymand, Alexander Keylin & Mehdi Ahmadian, "A survey of wheel–rail contact models for rail vehicles", *International Journal of Vehicle Mechanics and Mobility*, Vol. 54, (2016), No. 3, pp. 386–428.
- Qian Xiao, Jifeng Zheng, Jihua Liu and Jun Fang, "Analysis of the wheel/rail rolling contact fatigue of a high-speed train under the transient mechanism", *Journal of Mechanical Science and Technology*, Vol. 31 No. 5 (2017) pp. 2235-2242.
- Yeon-Sun Choi and Bum-Sik Shin, "Critical speed of high-speed trains considering wheel-rail contact", *Journal of Mechanical Science and Technology*, Vol. 29, No. 11 (2015), 4593-4600.
- Oldrich Polach and Dirk Nicklisch, "Wheel/Rail Contact Geometry Parameters in Regard to Vehicle Behaviour and their Alteration with Wear", *Wear an International Journal on the Science and Technology of Friction, Lubrication and Wear*, Accepted 28 th March, 2016 pp. 2-17.
- Roya Sadat Ashofteh and Ali Mohammadnia, "Stress Analysis in the Elastic-Plastic Analysis of Railway Wheels", *International Journal of Railway*, The Korean Society for Railway Vol. 7, No. 1 / March 2014, pp. 1-7
- Yuewei Ma, Valeri Markine, Abdul Ahad Mashal and Mingfa Ren, "Modeling verification and influence of operational patterns on tribological behavior of wheel-rail interaction", *Tribology International*, 114 (2017) pp. 264–281.
- R. Lewis and U. Olofsson, "Wheel-Rail Interface Handbook", Woodhead Publishing in Mechanical Engineering, 2009, pp. 58-92, 211-244.
- K. L. Johnson, "Contact Mechanics", Cambridge University Press, 1985, pp. 94-117.
- Timoshenko and J. N. Goodier, "Theory of Elasticity", McGraw Hill, 1951, pp. 343-398.
- Budynas-Nisbett, "Shigley's Mechanical Engineering Design", 8th Edition, McGraw-Hill, 2008, pp. 550-596.
- <http://www.nssmc.com/Nippon> Steel and Sumitomo Metal Corporation, Tokyo 2014, pp. 07.
- <http://www.ingexpert.com/PR NF EN 13715>, European Standard, 2015.

Appendix:

Table 1 Values of ‘m’ and ‘n’ for various values of θ .

θ °	30	35	40	45	50	55	60	65	70	75	80	85	90
m	2.73 1	2.39 7	2.13 6	1.92 6	1.75 4	1.61 1	1.48 6	1.37 8	1.28 4	1.20 2	1.12 8	1.06 1	1
n	0.49 3	0.53 0	0.56 7	0.60 4	0.64 1	0.67 8	0.71 7	0.75 9	0.80 2	0.84 6	0.89 3	0.94 4	1

(Source: Theory of elasticity by Timoshenko and J. N. Goodier [19])

Table 2 The effect of wheel profile taper on the contact dimension, maximum contact pressure and equivalent stress based on Hertzian contact calculation

WPT	a (mm)	b (mm)	σ_x (MPa)	σ_y (MPa)	σ_z (MPa)	HCT Result P_o (MPa)	HCT Result σ' (MPa)
1 in 5	7.4076	3.6709	-1067.6	-1264.2	-1457.4	1457.4	337.581
1 in 10	7.4410	3.6583	-1065.4	-1263.9	-1455.8	1455.8	338.112
1 in 15	7.4471	3.6557	-1065.1	-1263.9	-1455.7	1455.7	338.288
1 in 20	7.4496	3.6547	-1065.0	-1263.9	-1455.6	1455.6	338.289
1 in 25	7.4501	3.6547	-1064.9	-1263.9	-1455.5	1455.5	338.289
1 in 30	7.4511	3.6542	-1064.9	-1263.9	-1455.5	1455.5	338.29
1 in 35	7.4511	3.6542	-1064.9	-1263.9	-1455.5	1455.5	338.29

Table 3 The effect of radii of curvatures of wheel on the contact dimension, maximum contact pressure and equivalent stress based on Hertzian contact calculation and FEA

R_2^t	a (mm)	b (mm)	σ_x (MPa)	σ_y (MPa)	σ_z (MPa)	HCT Result P_o (MPa)	FEM Result P_o (MPa)	Difference in %	HCT Result σ' (MPa)	FEM Result σ' (MPa)	Difference in %
300	7.4960	3.5660	1080.7	1291.3	1482.5	1482.5	1471.6	0.74	348.10	342.19	1.7
310	7.4765	3.5805	1080.0	1288.7	1480.4	1480.4	1467	0.9	346.86	340.4	1.86
320	7.4616	3.6262	1070.4	1273.1	1464.7	1464.7	1457.5	0.49	341.52	337.1	1.29
330	7.4496	3.6547	1065.0	1264.0	1455.6	1455.6	1450.7	0.34	338.29	333.31	1.47
340	7.4371	3.6828	1059.8	1255.2	1446.9	1446.9	1446.9	0	335.24	333.2	0.61
350	7.4248	3.7093	1055.1	1247.2	1438.9	1438.9	1438	0.06	332.38	330.57	0.54
360	7.4126	3.7349	1050.7	1239.6	1431.4	1431.4	1415.3	1.12	329.67	324.28	1.63

Table 4 The effect of radii of curvatures of rail on the contact dimension, maximum contact pressure and equivalent stress based on Hertzian contact calculation and FEA

R_1^t	a (mm)	b (mm)	σ_x (MPa)	σ_y (MPa)	σ_z (MPa)	HCT Result P_o (MPa)	FEM Result P_o (MPa)	Difference in %	HCT Result σ' (MPa)	FEM Result σ' (MPa)	Difference in %
270	7.5085	3.5470	-1083.8	-1297.0	-1488.0	1488.0	1485.7	0.15	350.22	342.2	2.29
280	7.4849	3.5838	-1077.8	-1286.0	-1477.4	1477.4	1481.2	0.26	346.17	343.39	0.80
290	7.4648	3.6198	-1071.5	-1275.0	-1466.6	1466.6	1457.5	0.62	342.22	345.58	0.97
300	7.4496	3.6547	-1065.0	-1264.0	-1455.6	1455.6	1450.7	0.34	338.29	333.31	1.47
310	7.4339	3.6885	-1058.9	-1253.6	-1445.3	1445.3	1421.8	1.63	334.64	345.43	3.12
320	7.4189	3.7212	-1053.1	-1243.7	-1435.5	1435.5	1425.2	0.72	331.17	328.65	0.76
330	7.4042	3.7518	-1047.9	-1234.7	-1426.6	1426.6	1415.4	0.79	327.97	323.12	1.48